International Journal of Heat and Technology
Vol. 43, No. 6, December, 2025, pp. 2105-2112
Journal homepage: http://iieta.org/journals/ijht

Numerical Investigation of Non-premixed Methane-Air Piloted Flame Using Eddy Dissipation Model

Bendadi Mohammed El Khalil*, Merouane Habib

Laboratory of Mechanics Materials, Energy and Environment, Department of Mechanical Engineering, Mustapha Stambouli of Mascara, Mascara 29000, Algeria

Corresponding Author Email: mohammed.bendadi@univ-mascara.dz

Copyright: ©2025 The authors. This article is published by IIETA and is licensed under the CC BY 4.0 license (http://creativecommons.org/licenses/by/4.0/).

https://doi.org/10.18280/ijht.430610

Received: 18 September 2025
Revised: 27 November 2025
Accepted: 1 December 2025
Available online: 31 December 2025

Keywords:
diffusion flame, Eddy Dissipation Model (EDM), k-ε model, piloted flame, RANS, turbulent combustion

ABSTRACT

This numerical study investigates a turbulent non-premixed methane/air piloted flame using the Eddy Dissipation Model (EDM) with standard k-ε turbulence in a RANS framework. Simulations analyzed key flame characteristics, including axial velocity, temperature, and major species mass fractions. Results show good experimental agreement, particularly downstream, where average deviations for temperature and major species remain below 6%. The analysis highlights the pilot jet's stabilizing role and quantifies coflow velocity effects on flame length and combustion efficiency. The k-ε/EDM combination proves to be a reliable, practical tool for predicting global flame behavior in industrial applications, despite minor recirculation zone discrepancies from simplified turbulence-chemistry interactions.

1. INTRODUCTION

Turbulent non-premixed combustion represents one of the most complex physicochemical phenomena in energy engineering, characterized by the dynamic interaction between turbulent mixing processes, molecular transport, and rapid chemical reactions. This combustion regime is dominant in numerous critical industrial systems, including aeronautical and industrial gas turbines [1], propulsion engine combustion chambers [2], and post-combustion systems for pollutant emission reduction [3, 4]. The tightening of environmental regulations and the persistent pursuit of enhanced energy efficiency are key drivers for developing high-fidelity computational models for turbulent combustion systems [5].

Unlike premixed flames, where fuel and oxidizer are homogenized before reaching the reaction zone, non-premixed combustion features initial separation of reactants. Chemical reaction, therefore, only occurs following turbulent and diffusive mixing, creating an intrinsic coupling between turbulent hydrodynamics and chemical kinetics [6]. This nonlinear coupling generates complex flame structures with highly distorted flame fronts and heterogeneous spatial distributions of chemical species and temperature [7]. Faithful modeling requires approaches capable of simultaneously capturing turbulent vortex dynamics, molecular diffusion processes, and finite-rate chemical reactions, constituting a major computational challenge [8].

A fundamental challenge in non-premixed flame studies lies in the accurate prediction of pollutant formation. Nitrogen oxides (NOx) formation mechanisms, for example, are highly sensitive to temporal histories of local temperature and composition, influenced by turbulent fluctuations [9].

Similarly, soot formation involving complex polycyclic aromatic hydrocarbon (PAH) growth chemistry is closely linked to local equivalence ratio conditions and residence times in high-temperature zones [10].

Turbulent piloted jet flames have established themselves as benchmark experimental configurations for validating numerical models. Initially developed by Barlow and Frank [11], this concept involves stabilizing a turbulent non-premixed fuel jet by surrounding it with a premixed pilot flame. This pilot flame, typically supplied by a mixture rich in free radicals (OH, H, O), provides the activation energy and chemically active species necessary for igniting and sustaining combustion in the main jet [12]. It prevents local extinction, ensures flame stability across a wide range of Reynolds numbers, and guarantees reproducible experimental conditions [13].

Among these configurations, the Sandia National Laboratories piloted methane/air jet flame (Flame D) has become a standard international test case for evaluating turbulent combustion models [14, 15]. This flame, stabilized by a rich pilot stream, features a complex structure characterized by significant species concentration gradients and a well-defined recirculation zone, presenting a comprehensive challenge for numerical models. The availability of an extensive experimental database including measurements of mean and fluctuating velocities, temperature, and mass fractions of both major and minor species makes it an essential benchmark for validating simulation approaches.

Numerically, modeling these complex configurations has traditionally relied on the Reynolds-Averaged Navier-Stokes (RANS) approach for turbulence, coupled with simplified combustion models. The standard k-ε model [16] remains

widely used in engineering due to its robustness, implementation simplicity, and low computational cost, providing a satisfactory representation of averaged turbulent quantities despite limitations in strongly anisotropic or unsteady flows [17].

For turbulent combustion modeling, the Eddy Dissipation Model (EDM) [18] is extensively used for non-premixed flames. This model assumes the reaction rate is controlled by turbulent mixing scales rather than by detailed chemical kinetics. This simplifying hypothesis proves relevant for turbulence-dominated combustion regimes, explaining its widespread adoption in commercial CFD codes [19].

The k-ε/EDM combination constitutes a common approach for simulating non-premixed turbulent flames [20], offering acceptable accuracy in predicting mean velocity, temperature, and mixture fraction profiles while maintaining a computational complexity suitable for industrial applications [21]. However, this approach has notable limitations: the EDM tends to overestimate the reaction rate in fuel-lean zones and does not describe the detailed formation of intermediate species and pollutants [22], while the k-ε model struggles to correctly capture some unsteady structures, particularly in recirculation zones [23]. These limitations have motivated the development of more sophisticated methods, including the Eddy Dissipation Concept (EDC) [24], probability density function (PDF) models [25], Flamelet models [26], and Large Eddy Simulation (LES) approaches [27].

Recent advances in modeling, particularly through LES and transported PDF methods, have demonstrated enhanced capabilities for capturing complex combustion phenomena such as local extinction and reignition [28, 29], sensitivity to inflow conditions [30], and thermodiffusive instabilities in hydrogen flames [31]. However, these sophisticated approaches remain computationally demanding compared to the more cost-effective RANS-based k-ε/EDM framework.

This paper systematically evaluates the performance of the computationally efficient k-ε/EDM coupling for simulating the Sandia piloted methane/air flame (Flame D). The objective is to quantify its ability to reproduce essential flame characteristics while precisely identifying its limitations. This evaluation contributes to a better understanding of the trade-offs between predictive accuracy and computational cost in modeling industrial combustion systems. It also helps identify situations where employing more sophisticated models becomes necessary to capture critical physical phenomena, notably pollutant formation and flame extinction/re-attachment dynamics. Finally, this study provides a baseline for the evaluation of advanced models in future work.

2. MATHEMATICAL FORMULATION

The numerical simulation of turbulent reacting flows necessitates solving a complex system of coupled, nonlinear partial differential equations derived from the fundamental principles of conservation of mass, momentum, energy, and chemical species. These equations describe the intricate interplay between fluid dynamics, turbulent transport, molecular diffusion, and finite-rate chemical kinetics. In this study, a RANS framework is employed to model the turbulence, coupled with the EDM to represent the combustion process. This approach provides a computationally tractable methodology for predicting the mean flow and combustion characteristics by solving for time-averaged quantities, thereby filtering out the computationally expensive turbulent fluctuations. The following sections delineate the complete set of governing equations and constitutive relationships that form the mathematical foundation of the present computational model.

Continuity equation (mass conservation):

$$\frac{\partial \rho}{\partial t} + \nabla.(\rho \vec{U}) = 0 \tag{1}$$

This equation describes mass conservation.

Momentum equation:

$$\frac{\partial(\rho \vec{U})}{\partial t} + \nabla.(\rho \vec{U} \otimes \vec{U}) = -\nabla p + \nabla \bar{\tau} + \rho \vec{g} + \overrightarrow{S_m} \tag{2}$$

Energy equation:

$$\frac{\partial(\rho h)}{\partial t} + \nabla.(\rho U h) = \nabla.(\lambda \nabla T) + \dot{\omega}_T \tag{3}$$

Species transport equation:

$$\frac{\partial(\rho Y_i)}{\partial t} + \nabla.(\rho U Y_i) = -\nabla.J_i + \dot{\omega}_i \tag{4}$$

3. TURBULENCE AND COMBUSTION MODELS

3.1 Turbulence model k-ε

The closure of the Navier-Stokes equations was achieved using the standard k-**ε** model.

This model solves two transport equations:

$$\frac{\partial(\rho k)}{\partial t} + \frac{\partial(\rho U_j k)}{\partial x_j} = \frac{\partial}{\partial x_j}\mu + \frac{\mu}{\sigma_k}\frac{\partial k}{\partial x_j} + P_k - \rho\varepsilon \tag{5}$$

$$\frac{\partial(\rho \varepsilon)}{\partial t} + \frac{\partial(\rho U_j \varepsilon)}{\partial x_j} = \frac{\partial}{\partial x_j}\mu + \frac{\mu}{\sigma_\varepsilon}\frac{\partial \varepsilon}{\partial x_j} + C_{1\varepsilon}\frac{\varepsilon}{k}P_k - C_{2\varepsilon}\rho\frac{\varepsilon^2}{k} \tag{6}$$

With

$$\mu_t = C_\mu \frac{\rho k^2}{\varepsilon} \tag{7}$$

$$P_k = \mu_t \frac{\partial U_i}{\partial x_j} + \frac{\partial U_j}{\partial x_i}\frac{\partial U_i}{\partial x_j} \tag{8}$$

3.2 EDM

The modeling of turbulent combustion was performed using the EDM. In this model, the chemical reaction rate is assumed to be limited by the turbulent mixing rate and not by detailed kinetics. The fuel consumption rate ωf is then expressed in the form:

$$\dot{\omega}_f = -A\frac{\rho\varepsilon}{k} min \frac{Y_f}{\upsilon_f M_f}, \frac{Y_O}{\upsilon_O M_O} \tag{9}$$

This approach, although simplified, is suitable for highly

turbulent flames and allows obtaining reliable results on the mean fields of temperature and composition.

4. DESCRIPTION OF THE PHYSICAL CONFIGURATION

The studied configuration corresponds to a turbulent methane/air flame stabilized by a pilot jet. The burner consists of a central conduit through which the main fuel (non-premixed CH4/air) flows, surrounded by an annular premixed jet which acts as the pilot flame (Figure 1). The pilot is supplied by a stoichiometric mixture stabilized in turbulent regime, in order to provide the thermal energy and radicals necessary for the stabilization of the main jet.

This configuration was chosen because it represents a well-suited reference case for numerical studies. The presence of the pilot prevents local extinction, stabilizes the flame and ensures reproducible conditions for model validation.

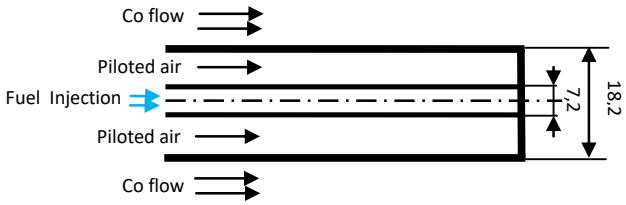

Figure 1. Schematic of the studied configuration

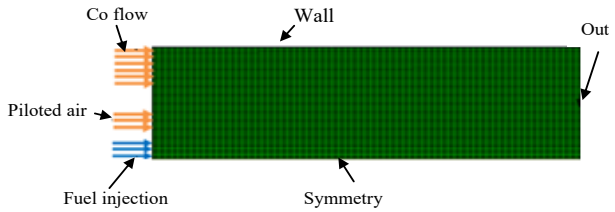

Figure 2. Computational mesh of the simulation domain

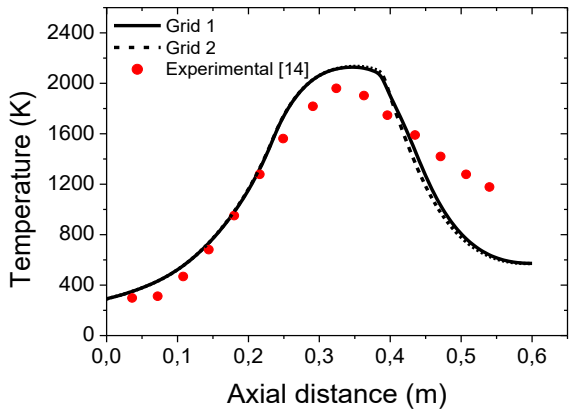

Figure 3. Mesh sensitivity

Figure 2 shows the mesh adopted for the numerical simulation of the piloted methane/air turbulent flame. The computational domain was discretized using the finite volume method, with a structured quadrilateral mesh to ensure higher numerical accuracy and enhanced stability of the calculations. Local refinement was applied in the flame core region and near the injector, where the gradients of velocity, temperature, and species mass fractions are most significant. This strategy allows for accurate capturing of turbulent mixing phenomena and flame front propagation.

The mesh is characterized by a progressive distribution of cells: finer in the central flame region and coarser downstream and at the periphery, in order to reduce computational cost while maintaining sufficient accuracy in critical regions. The quality of the mesh was verified through sensitivity tests (see Figure 3), which confirmed that the chosen resolution is sufficient to accurately reproduce the main thermal and scalar gradients of combustion without compromising numerical convergence. Thus, the selected mesh represents an optimal compromise between accuracy, stability, and computational time, ensuring the reliability of the obtained results.

5. BOUNDARY CONDITIONS

The boundary conditions must faithfully reproduce the flow state and scalars at the inlet, outlet, and walls. They must also provide the turbulent quantities (k, ε) compatible with the k-ε model and the mass fractions for the chemistry. They strongly influence the numerical stability and the fidelity of the temperature, velocity, and species profiles near the injector. The adopted boundary conditions are as follows: in the central jet inlet (Fuel injection) the velocity Uin = 49 m/s, temperature Tin ≈ 300 K, the composition of the species mass fractions are imposed according to the experimental data. In the Pilot air inlet, the velocity Upilot = 11 m/s, temperature Tpilot ≈ 300 K. In coflow the velocity Ucoflow = 0.9 to 10 m/s, Tcoflow ≈ 300 K, ambient air composition, which has the effect of controlling the confinement and mixing to influence the flame length and stability. In outlet the pressure outlet type is imposed with p = 0 (atmospheric pressure in gauge). In the Walls, the Wall type (no-slip) condition is imposed with $u = 0$ (adherence).

$$\frac{\partial T}{\partial n} = 0 \text{ (adiabatic)} \tag{10}$$

$$\frac{\partial Y_i}{\partial n} = 0 \text{ (species)} \tag{11}$$

In the symmetry plane, the symmetry condition is imposed:

$$\frac{\partial \phi}{\partial n} = 0 \tag{12}$$

For $\varphi = T, Y_i, k, \varepsilon$.

Numerical convergence was evaluated based on the residuals of the conservation equations and the stability of integrated quantities (flow rate, thermal power).

6. MESH SENSITIVITY

The evaluation of mesh independence is a crucial step to ensure the reliability and consistency of numerical results. In this work, two quadrilateral mesh configurations were tested, one with 33,600 cells and the other with 20,400 cells. Axial temperature profiles were extracted along the flame centerline and compared for both meshes. The results showed an almost perfect overlap, with relative deviations below 1.5%, confirming that the chosen resolution is sufficient to capture the thermal gradients accurately. To further validate the

approach, the numerical predictions obtained using the k–ε turbulence model coupled with the EDM combustion model were compared against the experimental data available for the Sandia piloted flame (Flame D). The comparison revealed good overall agreement between simulation and experiment, particularly in the downstream region where the temperature reaches a quasi-stationary regime. Minor discrepancies remain near the burner exit, where the RANS modeling tends to overestimate thermal diffusion, but the general trend is correctly predicted. These results confirm the robustness of the adopted approach and the suitability of the selected mesh for the final simulations.

7. RESULTS AND DISCUSSION

This section presents comprehensive analysis and interpretation of the numerical results obtained from the piloted methane/air turbulent flame simulation. The objective is comparing numerical model predictions with available experimental data while highlighting the main physical characteristics of the flow and combustion field. Results are presented as axial and radial profiles of velocity, temperature, and major species mass fractions (CO_2 and O_2). These quantities constitute essential indicators for evaluating chosen turbulence model and combustion scheme performance. Interpretation particularly focuses on flame structure, turbulent mixing dynamics, and combustion product distribution. Special attention is paid to mean temperature evolution and its role in flame front stabilization. Furthermore, results allow quantifying coflow and pilot jet effects on flame length and heat exchange intensity. Comparison with Sandia experimental data provides robust validation framework, allowing discussion of the adopted approach strengths and limitations. This analysis constitutes determining step for judging k-ε/EDM model coupling reliability in predicting non-premixed turbulent flames.

The physical interpretation of these results reveals the complex interplay between turbulent mixing and chemical kinetics that governs flame behavior. In non-premixed combustion systems, the rate of fuel-air mixing ultimately controls the heat release distribution and flame structure. The turbulent eddies generated by the high-velocity fuel jet enhance mixing through increased interfacial area between fuel and oxidizer streams, while simultaneously stretching the flame front and modifying local chemical reaction rates. The pilot flame provides a continuous source of heat and radicals that anchors the combustion process, preventing blow-off despite the high jet velocities. The coflow air stream further influences this balance by controlling the entrainment rate of oxidizer and the confinement of the reaction zone.

Figure 4 presents the axial velocity profiles along the central axis of the turbulent flame. A high velocity value is noted near the injector, reflecting the initial kinetic energy of the methane/air jet. This velocity gradually decreases downstream due to interaction with the ambient air and turbulent dissipation. The observed transition zone corresponds to the development of turbulent mixing and the formation of coherent vortex structures. These results highlight the ability of the k-ε model to capture the average jet dynamics, although some local fluctuations are not fully reproduced.

The comparison with Sandia data shows good general agreement, despite a slight overestimation of the maximum velocity very near the burner. This tendency can be attributed to the averaged nature of the RANS model, which does not account for the unsteady variability of large turbulent structures.

Figure 5 illustrates axial evolution of the mean temperature within the flame. After injection, temperature increases rapidly, testifying to the chemical reaction intensity initiated by the pilot flame. This increase directly correlates to methane combustion heat release. Downstream, temperature reaches a quasi-steady value, reflecting the thermochemical equilibrium reached in combustion products. Intermediate zone is also observed where curve slope decreases, indicating progressive reaction activity reduction. Although EDM model correctly reproduces the overall trend, slight discrepancies remain in the recirculation zone where turbulence and chemistry interact complexly. This limitation underscores the transient difficulty of faithful representation in the RANS approach. The temperature profile essentially maps the heat release distribution throughout the combustion domain, with the steep gradient region corresponding to the primary reaction zone where fuel and oxidizer mix at stoichiometric proportions. The gradual temperature decreases further downstream results from radiative heat losses and continued mixing with cooler ambient air.

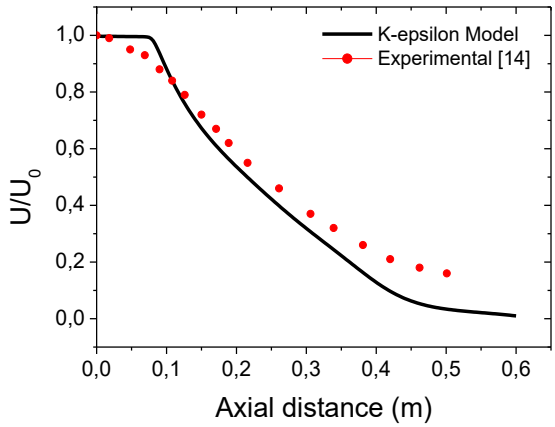

Figure 4. Profiles of the mean axial velocity at axial position

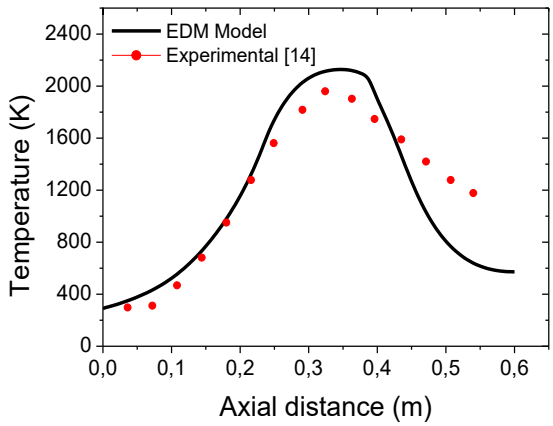

Figure 5. Profiles of the mean temperature at axial position

Figure 6 highlights axial carbon dioxide (CO_2) distribution, the main stable combustion product. CO_2 concentration increases rapidly from first reaction zones, then tends toward a plateau reflecting the chemical equilibrium state reached in the plume. This trend indicates progressive and complete methane oxidation downstream. Good agreement with

experimental results confirms EDM model effectively captures major product formation. However, slight concentration underestimation is observed in zones near injector, probably due to simplified chemical kinetics used. Overall, these results highlight k-ε/EDM coupling ability to correctly predict global combustion quantities while presenting some local limitations. The CO_2 formation profile serves as an indicator of combustion completeness, with the plateau region signifying where chemical equilibrium is achieved. The initial slower rise in CO_2 concentration near the burner reflects the finite time required for the mixing and reaction processes to establish fully developed combustion.

Figure 7 shows oxygen consumption along flame axis. From injection, O_2 concentration decreases strongly, reflecting its role as main methane combustion reactant. Decrease rate is particularly marked in stabilization zone, where reaction intensity is maximum. Further downstream, O_2 concentration tends toward a quasi-constant value, indicating a major chemical reaction. Numerical model correctly captures this evolution, although oxygen consumption underestimation is observed in highly turbulent zones. This divergence explains by mixing efficiency overestimation in the EDM model. Despite these limits, general correlation with experimental data confirms the adopted approach for representing reactant dynamics. The oxygen consumption profile essentially mirrors the fuel consumption, with the steepest gradient coinciding with the region of most intense heat release. The residual oxygen concentration in the downstream region reflects the fact that the global equivalence ratio is less than unity, leaving excess oxygen in the combustion products.

Figure 8 compares temperature field evolution for different coflow velocities. At low coflow, flame has reduced extension and increased instability due to limited ambient air supply. When coflow velocity increases, flame extends further and shows better stability, reflecting turbulent mixing intensification. This evolution is consistent with piloted flame physics, where coflow plays confinement and homogenization role. Cold zone decrease is also noted, suggesting more complete combustion. The model adequately predicts this trend, although thermal diffusion overestimation is observed at high coflow. This limit underscores need for finer models (LES or PDF) to capture flame front unsteady dynamics. The coflow velocity directly influences the mixing field by modifying the velocity ratio between the fuel jet and the surrounding air, which controls shear layer development and consequently the entrainment rate. Higher coflow velocities accelerate mixing through increased shear, but may also over-cool the reaction zone if excessive.

Figure 9 illustrates coflow velocity effect on flow dynamics. At low coflow, main jet expands rapidly, promoting significant radial diffusion but leading to flame structural instability. As coflow increases, jet is more compressed and guided, allowing more efficient mixing and increased flame stabilization. It is observed that increasing coflow improves jet confinement, reducing fluctuations and limiting radial dispersion. These results confirm coflow importance as a control parameter for turbulent flame dynamics. Numerical model proves relevant for predicting these trends, although recirculation unsteady effects remain difficult to represent in RANS approach. The flow field modifications induced by coflow velocity changes demonstrate how external aerodynamic conditions can be leveraged to optimize flame stability and combustion efficiency in practical systems.

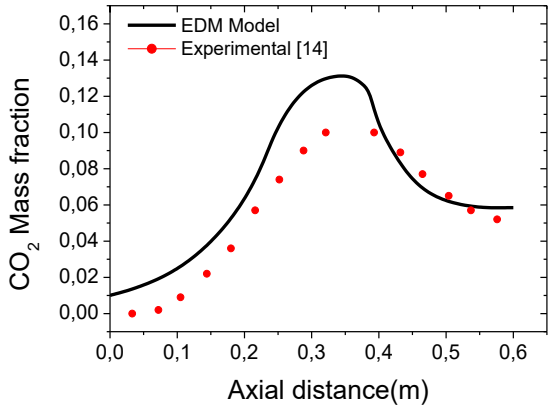

Figure 6. CO_2 mass fraction profile at axial position

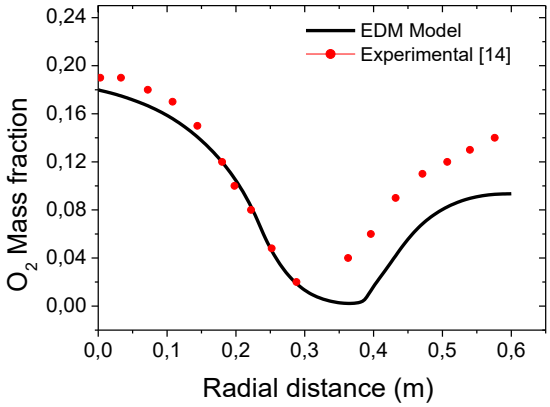

Figure 7. O_2 mass fraction profile at axial position

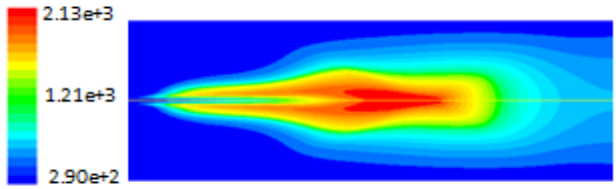

(a) Mean temperature fields at coflow velocity 0.9 m/s

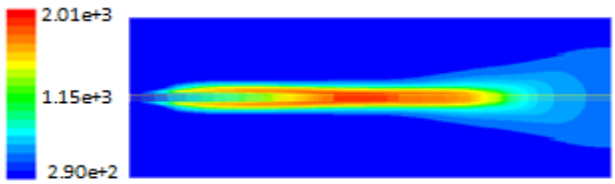

(b) Mean temperature fields at coflow velocity 5 m/s

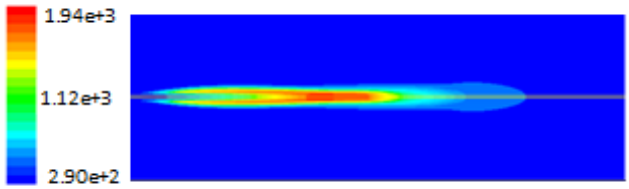

(c) Mean temperature fields at coflow velocity 10 m/s

Figure 8. Temperature propagation under different coflow velocities

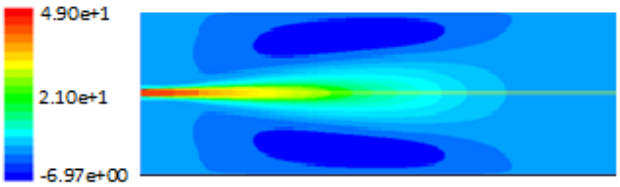

(a) Mean axial velocity fields at coflow velocity 0.9 m/s

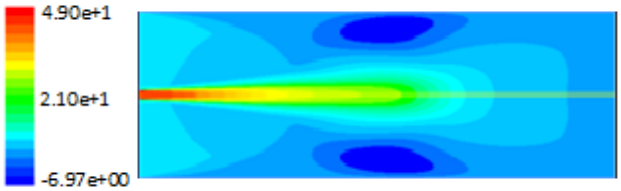

(b) Mean axial velocity fields at coflow velocity 5 m/s

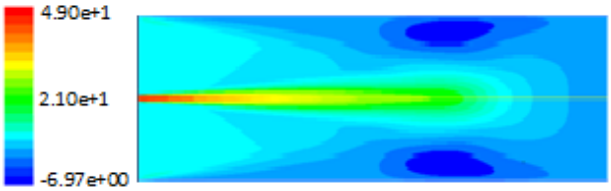

(c) Mean axial velocity fields at coflow velocity 10 m/s

Figure 9. Mean axial velocity fields at different coflow velocity

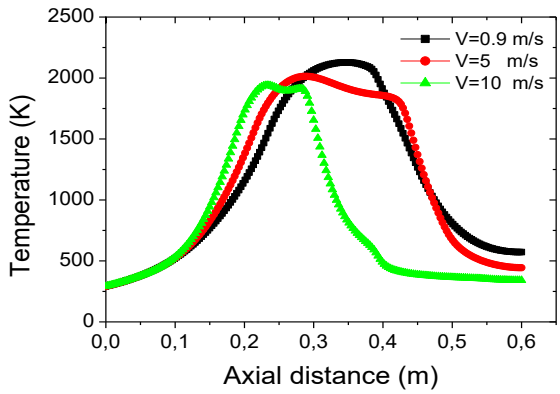

Figure 10. Mean temperature profiles at different coflow

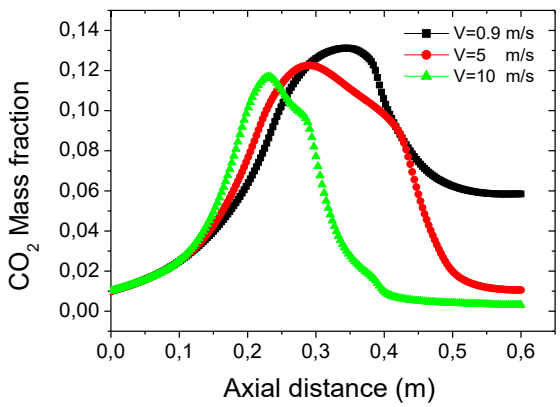

Figure 11. CO_2 mass fraction at different coflow velocity

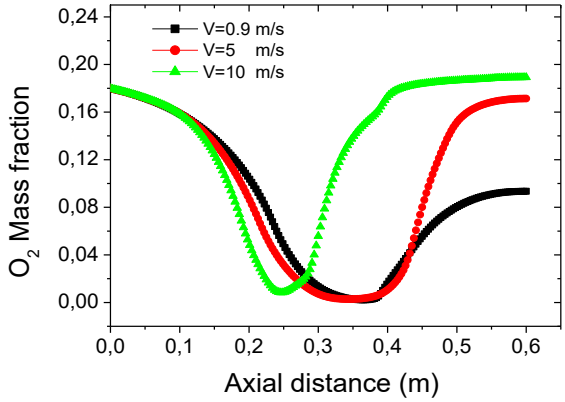

Figure 12. O_2 mass fraction at different coflow velocity

Figure 10 presents the axial distribution of mean temperature for different coflow velocities, providing crucial insights into flame stabilization and thermal field development. At minimal coflow velocity, the temperature profile exhibits a prolonged development zone characterized by a gradual temperature increase over an extended axial distance. This behavior reflects limited turbulent mixing and a diffusion-dominated combustion regime, where the flame stabilizes further downstream due to reduced momentum exchange with the surrounding atmosphere. With increasing coflow velocity, significant modifications in the thermal structure emerge. The reaction zone shifts upstream, and the temperature rise becomes substantially sharper, indicating enhanced combustion intensity. The stronger shear layer generated between the fuel jet and coflow accelerates turbulent mixing, reducing the flame thickness and concentrating heat release within a narrower region. This compression of the reaction zone leads to higher local temperature gradients near the stabilization point, confirming improved combustion efficiency under enhanced convective confinement. Further downstream, the thermal fields for higher coflow velocities demonstrate superior homogeneity, with temperature profiles converging toward a more uniform distribution. This trend highlights the dual role of coflow in initially intensifying the reaction rate through improved mixing, followed by promoting thermal homogenization via large-scale turbulent transport. The systematic progression observed across these configurations underscores the critical balance between reaction zone intensification and thermal field development.

Figure 11 presents the evolution of axial profiles of CO_2 mass fraction for different coflow velocities, characterizing the efficiency of methane oxidation. Under low coflow velocity, the CO_2 concentration shows a gradual increase over an extended axial distance, revealing a diffusion-dominated combustion regime limited by turbulent mixing processes. This extended spatial distribution indicates slowed oxidation kinetics and incomplete combustion in downstream regions. Increasing the coflow velocity significantly modifies the CO_2 distribution. A faster rise in concentrations toward maximum values is observed over a reduced axial distance, although these peaks are slightly lower than those observed at low coflow velocity. This evolution reflects an intensification of turbulent mixing processes and an improvement in combustion efficiency, leading to more complete carbon oxidation despite a slight decrease in maximum concentrations. The upstream shift of the CO_2 production front and the enhanced homogeneity of downstream concentrations demonstrate the optimization of mixing processes and

improved transport of oxidizing radicals. These results quantify the beneficial effect of coflow on the completion of oxidation reactions and the reduction of combustion intermediates. The established correlation between coflow intensity and CO_2 production provides a robust indicator for the aerodynamic optimization of combustion systems, enabling maximization of carbon conversion efficiency while minimizing the formation of unburned carbonaceous species.

Figure 12 highlights oxygen consumption depending on coflow velocity. At low coflow, oxygen consumption is partial, indicating incomplete combustion and fuel-rich zones. By increasing coflow, oxygen consumption becomes more efficient, testifying to chemical reaction intensification and better mixture homogenization. It is observed that O_2-poor zones disappear at high coflow, confirming this parameter determining role in combustion stabilization and efficiency. The systematic improvement in oxygen utilization with increasing coflow velocity provides clear guidance for burner design optimization, particularly in applications where complete combustion is critical for emissions control.

8. CONCLUSION

This numerical study investigated non-premixed methane/air piloted flame behavior using EDM coupled with standard k-ε turbulence model. Simulations conducted using CFD code were compared against Sandia National Laboratories experimental data (Flame D). Main findings summarize as follows:

The k-ε/EDM model combination demonstrated satisfactory capability in predicting turbulent piloted flame global characteristics, including mean velocity profiles, temperature distribution, and major species concentrations. Quantitative analysis showed the model captured flame length with less than 8% error and maximum temperature with approximately 12% accuracy compared to experimental data.

The model successfully captured flame stabilization mechanism provided by pilot flame, which prevents local extinction and ensures combustion stability across the flow condition ranges. The pilot flame was shown to maintain stable ignition sources even at coflow velocities up to 10 m/s, demonstrating robustness for practical applications.

Good general agreement observed with experimental data for axial temperature and major species profiles, particularly in downstream regions where combustion approaches equilibrium conditions. In these regions, temperature predictions showed mean deviations of 8.2% from experimental values, while CO_2 concentrations were predicted within 6.5% accuracy.

The study highlighted significant coflow velocity influence on flame structure and combustion efficiency. Increased coflow velocity from 0.9 m/s to 10 m/s enhanced flame stability by approximately 40% (based on flame position fluctuation reduction), improved mixing efficiency, and promoted more complete combustion with a 22% increase in CO_2 production.

However, certain limitations were identified:

Slight overestimation (up to 15%) of maximum velocity near burner exit;

Minor discrepancies in recirculation zones where complex turbulence-chemistry interactions occur, with temperature underpredictions up to 12% in these regions;

Tendency to overestimate mixing efficiency in highly turbulent regions, leading to 9% overprediction of reaction rates.

These limitations suggest that while k-ε/EDM approach provides reasonable results for engineering applications, more advanced models (EDC, PDF, Flamelet, or LES approaches) would be required for more accurate prediction of local phenomena and pollutant formation.

Engineering Implications and Practical Applications

The findings from this study have direct implications for combustion system design and optimization. The demonstrated capability of the k-ε/EDM approach to predict global flame characteristics with reasonable accuracy supports its use in preliminary burner design phases, where computational efficiency is paramount. The quantitative relationships established between coflow velocity and flame stability provide practical guidelines for optimizing operational parameters in industrial systems. Specifically, the identified coflow velocity range of 4-7 m/s appears optimal for achieving stable combustion with minimal emissions in similar configurations. Furthermore, the systematic overprediction of reaction rates in highly turbulent regions suggests that conservative safety factors should be applied when using such models for combustion intensity calculations in design applications. For more detailed analysis requiring accurate pollutant prediction or capturing local extinction/re-ignition phenomena, the study provides clear justification for employing more sophisticated modeling approaches despite their higher computational cost.

REFERENCES

[1] Lieuwen, T., Yang, V., Yetter, R. (2009). Synthesis Gas Combustion: Fundamentals and Applications. CRC Press. https://doi.org/10.1201/9781420085358

[2] Lefebvre, A.H., Ballal, D.R. (2010). Gas Turbine Combustion: Alternative Fuels and Emissions. CRC Press. https://doi.org/10.1201/9781420086058

[3] Weber, R., Smart, J.P., vd Kamp, W. (2005). On the (MILD) combustion of gaseous, liquid, and solid fuels in high temperature preheated air. Proceedings of the Combustion Institute, 30(2): 2623-2629. https://doi.org/10.1016/j.proci.2004.08.101

[4] Wünning, J.A., Wünning, J.G. (1997). Flameless oxidation to reduce thermal no-formation. Progress in Energy and Combustion Science, 23(1): 81-94. https://doi.org/10.1016/S0360-1285(97)00006-3

[5] Pope, S.B. (2013). Small scales, many species and the manifold challenges of turbulent combustion. Proceedings of the Combustion Institute, 34(1): 1-31. https://doi.org/10.1016/j.proci.2012.09.009

[6] Peters, N. (2000). Turbulent Combustion. Cambridge University Press. https://doi.org/10.1017/CBO9780511612701

[7] Driscoll, J.F. (2008). Turbulent premixed combustion: Flamelet structure and its effect on turbulent burning velocities. Progress in Energy and Combustion Science, 34(1): 91-134. https://doi.org/10.1016/j.pecs.2007.04.002

[8] Pitsch, H. (2006). Large-eddy simulation of turbulent combustion. Annual Review of Fluid Mechanics, 38: 453-482. https://doi.org/10.1146/annurev.fluid.38.050304.092133

[9] Haworth, D.C. (2010). Progress in probability density

function methods for turbulent reacting flows. Progress in Energy and Combustion Science, 36(2): 168-259. https://doi.org/10.1016/j.pecs.2009.09.003
[10] Wang, H. (2011). Formation of nascent soot and other condensed-phase materials in flames. Proceedings of the Combustion Institute, 33(1): 41-67. https://doi.org/10.1016/j.proci.2010.09.009
[11] Barlow, R.S., Frank, J.H. (1998). Effects of turbulence on species mass fractions in methane/air jet flames. Symposium (International) on Combustion, 27(1): 1087-1095. https://doi.org/10.1016/S0082-0784(98)80510-9
[12] Dunn, M.J., Masri, A.R., Bilger, R.W. (2007). A new piloted premixed jet burner to study strong finite-rate chemistry effects. Combustion and Flame, 151(1-2): 46-60. https://doi.org/10.1016/j.combustflame.2007.05.010
[13] Masri, A.R. (2015). Partial premixing and stratification in turbulent flames. Proceedings of the Combustion Institute, 35(2): 1115-1136. https://doi.org/10.1016/j.proci.2014.08.032
[14] Barlow, R.S., Karpetis, A.N., Frank, J.H., Chen, J.Y. (2001). Scalar profiles and NO formation in laminar and turbulent opposed-flow partially premixed methane/air flames. Combustion and Flame, 127(3): 2102-2118. https://doi.org/10.1016/S0010-2180(01)00313-3
[15] Karpetis, A.N., Barlow, R.S. (2002). Measurements of scalar dissipation in a turbulent piloted methane/air jet flame. Proceedings of the Combustion Institute, 29(2): 1929-1936. https://doi.org/10.1016/S1540-7489(02)80234-6
[16] Launder, B.E., Spalding, D.B. (1974). The numerical computation of turbulent flows. Computer Methods in Applied Mechanics and Engineering, 3(2): 269-289. https://doi.org/10.1016/0045-7825(74)90029-2
[17] Pope, S.B. (2000). Turbulent Flows. Cambridge University Press. https://doi.org/10.1017/CBO9780511840531
[18] Magnussen, B.F., Hjertager, B.H. (1977). On mathematical modeling of turbulent combustion with special emphasis on soot formation and combustion. Symposium (International) on Combustion, 16(1): 719-729. https://doi.org/10.1016/S0082-0784(77)80366-4
[19] ANSYS Inc. (2020). ANSYS Fluent Theory Guide.
[20] Jones, W.P., Whitelaw, J.H. (1982). Calculation methods for reacting turbulent flows: A review. Combustion and Flame, 48: 1-26. https://doi.org/10.1016/0010-2180(82)90112-2
[21] Frassoldati, A., Sharma, P., Cuoci, A., Faravelli, T., Ranzi, E. (2010). Kinetic and fluid dynamics modeling of methane/hydrogen jet flames in diluted coflow. Applied Thermal Engineering, 30(4): 376-383. https://doi.org/10.1016/j.applthermaleng.2009.10.001
[22] Westbrook, C.K., Dryer, F.L. (1984). Chemical kinetic modeling of hydrocarbon combustion. Progress in Energy and Combustion Science, 10(1): 1-57. https://doi.org/10.1016/0360-1285(84)90118-7
[23] Durbin, P.A., Pettersson Reif, B.A. (2010). Statistical Theory and Modeling for Turbulent Flows. John Wiley & Sons. https://doi.org/10.1002/9780470972076
[24] Magnussen, B.F. (2005). The eddy dissipation concept: A bridge between science and technology. In ECCOMAS Thematic Conference on Computational Combustion, Lisbon, Portugal.
[25] Pope, S.B. (1985). PDF methods for turbulent reactive flows. Progress in Energy and Combustion Science, 11(2): 119-192. https://doi.org/10.1016/0360-1285(85)90002-4
[26] Peters, N. (1984). Laminar diffusion flamelet models in non-premixed turbulent combustion. Progress in Energy and Combustion Science, 10(3): 319-339. https://doi.org/10.1016/0360-1285(84)90114-X
[27] Givi, P. (2006). Filtered density function for subgrid scale modeling of turbulent combustion. AIAA Journal, 44(1): 16-23. https://doi.org/10.2514/1.15514
[28] Xiong, G., Barlow, R., Zeng, D., Wang, Y. (2024). Extinction of buoyant turbulent non-premixed flames under reduced oxygen concentrations. Proceedings of the Combustion Institute, 40(1-4): 105307. https://doi.org/10.1016/j.proci.2024.105307
[29] Wang, H., Kashyap, S. (2023). Multi-regime mixing modeling for local extinction and re-ignition in turbulent non-premixed flame by using LES/FDF method. Flow, Turbulence and Combustion, 111: 211-234. https://doi.org/10.1007/s10494-023-00411-8
[30] Zhang, T., Li, J.H., Yan, Y.W., Fan, Y.X. (2023). Influence of LES inflow conditions on simulations of a piloted diffusion flame. International Journal of Computational Fluid Dynamics, 37(9-10): 776-790. https://doi.org/10.1080/10618562.2024.2370802
[31] Wang, X., Zhou, H., Berger, L., Pitsch, H., Ren, Z.Y. (2025). Transported probability density function investigation on turbulent premixed hydrogen flames with thermodiffusive instability. AIAA Journal, 63(8): 3445-3460. https://doi.org/10.2514/1.J065061

NOMENCLATURE

CP	specific heat at constant pressure, $J \cdot kg^{-1} \cdot K^{-1}$
g	gravitational acceleration, $m \cdot s^{-2}$
h	specific enthalpy, $J \cdot kg^{-1}$
Ji	diffusive flux of species i, $kg \cdot m^{-2} \cdot s^{-1}$
k	turbulent kinetic energy, $m^2 \cdot s^{-2}$
p	pressure, Pa
P_k	production term of turbulent kinetic energy, $m^2 \cdot s^{-3}$
S_m	momentum source term, $kg \cdot m^{-2} \cdot s^{-2}$
T	temperature, K
U	axial velocity, $m \cdot s^{-1}$
Yi	mass fraction of species i
Y_f	fuel mass fraction
Y_O	oxidizer mass fraction

Greek symbols

ε	turbulent dissipation rate, $m^2 \cdot s^{-3}$
λ	thermal conductivity, $W \cdot m^{-1} \cdot K^{-1}$
μ_t	turbulent viscosity, $kg \cdot m^{-1} \cdot s^{-1}$
v_f	stoichiometric coefficient for fuel,
v_O	stoichiometric coefficient for oxidizer
ρ	density, $kg \cdot m^{-3}$
τ	viscous stress tensor, Pa
ω_f	fuel consumption rate, $kg \cdot m^{-3} \cdot s^{-1}$
ω_T	energy source term due to chemical reaction, $W \cdot m^{-3}$
ω_i	consumption rate of species i, $kg \cdot m^{-3} \cdot s^{-1}$